Available online at www.sciencedirect.com
SCIENCE DIRECT®
Diamond and Related Materials 13 (2004) 561–568
DIAMOND AND RELATED MATERIALS
www.elsevier.com/locate/diamond

Improved characterisation of C_2 and CH radical number density distributions in a DC arc jet used for diamond chemical vapour deposition

C.J. Rennick[a], A.G. Smith[a], J.A. Smith[a], J.B. Wills[a], A.J. Orr-Ewing[a], M.N.R. Ashfold[a,*], Yu.A. Mankelevich[b], N.V. Suetin[b]

[a]*School of Chemistry, University of Bristol, Bristol BS8 1TS, UK*
[b]*Nuclear Physics Institute, Moscow State University, 119899 Moscow, Russia*

Abstract

Modelling studies of the plasma chemistry prevailing in $CH_4/H_2/Ar$ mixtures in a DC arc jet reactor used for diamond chemical vapour deposition are reported, together with complementary new experimental data. Gas temperatures, T_{gas}, close to the substrate have been determined via analysis of the measured rotational state population distribution in $C_2(a)$ radicals and found to be $\sim$3200 K—similar to the temperature established previously in the free plume region. These, and previous (J. Appl. Phys. 92 (2002) 4213), T_{gas} and number density measurements are in good accord with the first results from a full 2D (r, z) modelling of the plasma chemical transformations and heat and mass transfer processes within the evolving plume and the periphery of the reaction chamber. The modelling shows formation of a shock front in the supersonic expansion, a few millimeters downstream from the nozzle exit. The spatial distributions of the various species number densities are predicted to display localised maxima and minima within the reaction chamber, reflecting the complex balance between gas flow, diffusive transfer and chemical transformations in the widely varying range of local conditions (notably T_{gas} and the H and H_2 concentrations). The calculations provide clear evidence of the importance of gas flow re-circulation in transporting the hydrocarbon feedstock gas (methane) from the injection ring to the hot plume. C_2H_2, C_2H, C, CH, C_2 and C_3 species are all predicted to be present at number densities $>5\times10^{12}$ cm^{-3} in the plume incident on the substrate; it is suggested that all of the major C containing radical species (i.e. most notably C_2H, C, CH, C_2 and C_3) must make some contribution to material growth in order to satisfy the experimentally measured film deposition rate.

Keywords: DC arc jet; H/C chemistry; 2D modelling; Cavity ring down spectroscopy

1. Introduction

DC arc jet plasmas operating with $CH_4/H_2/Ar$ gas mixtures enable chemical vapour deposition (CVD) of diamond films at rates that far exceed those achievable in most other reactor environments [1]. We have recently reported spatially resolved C_2 and CH number densities and gas temperatures in such arc jet activated gas mixtures [2]. For future reference, a schematic of our experimental arrangement is shown as an inset in Fig. 1. Radical detection involved use of cavity ring down spectroscopy (CRDS) [3,4]—a very sensitive, multi-pass absorption method that, in the present set-up, was used to obtain radially (r) averaged species column densities and gas temperatures, as a function of distance from the substrate (z) and process conditions (e.g. input power, gas mixing ratios, pressure, etc.). Conversion to number densities required assumptions about the radial distribution of radical density and gas temperature in the column separating the cavity mirrors. Our earlier analysis [2] was guided by the results of optical emission spectroscopy studies of the same arc jet plume, which showed emission from electronically excited $C_2(d)$ radicals to be localised within a $\sim$10 mm column width centred on the plume axis [5]. Radical number densities in the plume were thus estimated by assuming 'top-hat' shaped concentration and temperature distributions centred at approximately $r=0$. Similar approximations were employed in our initial quasi one-dimensional (1D)

*Corresponding author. Tel.: +44-117-9288312; fax: +44-117-9250612.
E-mail address: mike.ashfold@bris.ac.uk (M.N.R. Ashfold).

0925-9635/04/$ - see front matter © 2003 Elsevier B.V. All rights reserved.
doi:10.1016/j.diamond.2003.11.060

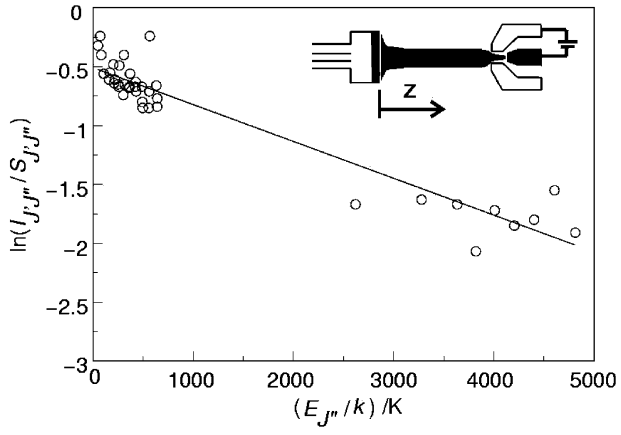

Fig. 1. $C_2(d \leftarrow a)$ (0, 0) absorption line intensity data measured at $z = 2$ mm, displayed in the form of a Boltzmann plot of $(I_{J',J''}/S_{J',J''})$ against $E_{J''}/k$, with $I_{J',J''}$ and $S_{J',J''}$, respectively, the measured intensity and calculated line strength of the spectral line connecting levels of the d- and a-states with rotational quantum numbers J' and J'', and $E_{J''}$ the calculated rotational energy of the J'' level in the $a^3\Pi_u$ ($v = 0$) state. The gradient of the best-fit line yields $T_{rot} = 3200 \pm 700$ K as the rotational temperature of the $C_2(a)_{v=0}$ radicals in the gas plume (averaged along the line-of-sight of the absorption measurement). The inset shows a schematic of the experimental apparatus defining the coordinate system employed in this work.

modelling of the evolving gas phase chemistry and composition as the plume evolves along z—i.e. from the output nozzle, through the expansion region and into the free stream region before encountering the substrate surface; 2D effects (e.g. radial diffusion and re-circulation) were incorporated within these simulations in an approximate manner only, using various plausible fitting functions [6].

Here, we present further results from a combined experimental and modelling study of the plasma chemistry prevailing in the Bristol DC arc jet reactor. Details of the 10 kW DC arc jet reactor operated with $CH_4/H_2/Ar$ mixtures and of the CRDS radical detection scheme for $C_2(a)$ and $CH(X)$ radicals have been presented previously [2,7]. New experimental findings introduced here include further investigations of the gas temperature in the immediate vicinity of the substrate, as revealed by measurements of the rotational state population distribution in the $C_2(a)$ radicals and a re-appraisal of the interpretation of individual Doppler broadened lineshapes. These, and previous measurements are compared with, and shown to be in very good accord with, first results from a full 2D (r, z) modelling study of the plasma chemical transformations, and heat and mass transfer processes both within the evolving plume and in the periphery of the reaction chamber. The simulations show formation of a shock in the supersonic jet, 6 mm downstream from the source exit, in accord with theoretical predictions [8]. The spatial distributions of species concentrations within the reaction chamber are predicted to exhibit local maxima and minima, as a result of the complex balance between gas flow, diffusive transfer and chemical transformations in a widely varying range of local conditions (most notably the gas temperature, T_{gas} and the H and H_2 concentrations). The calculated results provide very clear evidence of the importance of gas flow re-circulation in transporting the hydrocarbon feedstock gas (methane) from the injection ring to the hot plume.

2. Experimental results

As before [2], spectra of $C_2(a)$ radicals in the arc jet plume were recorded via the $d^3\Pi_g - a^3\Pi_u$ Swan band system over the wavenumber range 19 340–19 800 cm^{-1}. Individual absorption lines were assigned using the spectral simulation program PGOPHER [9], together with an N^2 Hamiltonian and literature values for the relevant ground and excited state spectroscopic constants [10,11]. Intensities, $I_{J',J''}$, of isolated rotational lines were integrated across the full line profile by fitting to Gaussian functions and used (together with absorption line strengths, $S_{J',J''}$, computed from the PGOPHER simulation) to construct Boltzmann plots of $\ln(I_{J',J''}/S_{J',J''})$ against $E_{J''}/k$ (where $E_{J''}$ is the rotational energy in the $C_2(a)$ radical) from which a rotational temperature, T_{rot}, can be estimated. Such T_{rot} values are necessarily an average along the line of sight of the absorption measurements and contain contributions from both the hotter central core of the arc jet and the cooler outer regions. Nonetheless, as shown in our previous measurements of $C_2(a)$ radicals in the free plume ($z > 5$ mm) [2], such plots appear reasonably linear over a wide range of $E_{J''}$. The average rotational temperature so derived for $z > 5$ mm was 3300 ± 200 K—in very good accord with translational temperatures derived from the full width half maxima (FWHM) of the Doppler broadened lineshape measured at the same z. Gas temperatures at smaller z have hitherto been estimated by linewidth measurements only. Such measurements are much less time consuming, experimentally, but are of lower precision both because of the rather weak ($T^{1/2}$) dependence of Doppler shift on T_{gas} and because of the need to deconvolute the (non-negligible) contribution that the bandwidth of the exciting laser makes to the measured FWHM value. Our previous lineshape measurements suggested that T_{gas} increases to values ~ 4500 K close to the substrate but, as Fig. 1 shows, a Boltzmann plot derived from an extensive $C_2(d-a)$ spectrum recorded along the column centred at $z = 2$ mm yields a T_{rot} value that agrees, within the experimental uncertainty, with the values measured at larger z. The laser beam waist in the centre of the optical cavity used here is estimated to be ~ 0.75 mm (diameter). This defines the experimental spatial resolution (along z). Attempts at measuring $C_2(d-a)$ CRD spectra at yet smaller z were

hampered by turbulence in the boundary layer and sporadic delamination of solid material from the substrate surface. As discussed below, the 2D modelling reveals that much of the additional linewidth measured at small z is attributable to deflection of the plasma flow velocity (initially along z) by the substrate into the plane normal to z, thereby increasing the measured Doppler width of a transition probed along r.

3. 2D (r, z) model of the DC arc jet plume

We have developed a self-consistent 2D (r, z) model of a DC arc discharge CVD reactor, specifically tailored to the Bristol DC arc jet reactor. The complete model comprises three blocks, describing (i) activation of the reactive mixture (i.e. gas heating, ionisation, molecular H_2 dissociation in the DC arc jet and intermediate chamber, H atom loss and production of molecular H_2 on the wall of the nozzle exit), (ii) gas-phase processes (heat and mass transfer, and chemical kinetics) and (iii) gas-surface processes at the substrate [6,12]. Thermochemical data and the reduced chemical reaction mechanism used were taken from Ref. [6]. The chemical kinetics scheme involved 23 species (H, H_2, Ar, C, CH, $^3CH_2$, $^1CH_2$, CH_3, CH_4, $C_2(X)$, $C_2(a)$, C_2H_x ($x=1$–6), C_3H_x ($x=0$–2), C_4H_x ($x=0$–2)) and 76 reversible reactions. The set of conservation equations for mass, momentum, energy and species concentrations, together with appropriate initial and boundary conditions, thermal and caloric equations of state, are integrated numerically in the cylindrical (r, z) coordinate space used to approximate the reaction chamber until attaining steady state conditions. The model output includes spatial distributions of T_{gas}, the flow field, and the various species number densities as a function of parameters like H_2 and CH_4 flow rates and input power.

Using published theory [13] for gas expansion into a low pressure chamber and our typical DC arc discharge conditions (gas flow rates of 11.4 slm Ar and 1.8 slm H_2, reaction chamber pressure $P=50$ Torr and input powers $\sim$6.5 kW), we estimate the following gas flow parameters at the exit of the output nozzle of the N-torch head: gas pressure, $P_L=862.5$ Torr, gas temperature, $T_{gas}=11\,000$ K and gas velocity, $v_L=2.3$ km s^{-1} (local sound velocity). The reaction chamber is modelled as two cylinders in series, with respective diameters of 5.5 and 10 cm, and lengths of 8 and 9 cm, respectively, and the substrate diameter was set at 2.6 cm. The dimensions of the second cylinder are smaller than those of the actual reactor (to reduce the computational time). They are large enough to span the actual diameter of the CH_4 injection ring and to reproduce the true nozzle to substrate separation but, inevitably, the reduced diameter will affect details of the gas transport and flow.

The specific input energy for our base set of the parameters is approximately 6.5 eV per atom. Measurements of Balmer-α emission intensities as a function of H_2 flow rate, together with approximate 1D model calculations, suggest an estimated degree of ionisation $\sim$10%. The 1D calculations indicate that charged species have little effect on the concentrations of neutral species within the plume, so charged species are not considered in the present 2D calculations. At the input powers used, almost all H_2 molecules are dissociated in the intermediate chamber within the N-torch head, by thermal dissociation Eq. (1)

$$H_2 + M \rightarrow 2H + M, \quad M = Ar,\ H_2 \tag{1}$$

and via the ion conversion reaction

$$Ar^+ + H_2 \rightarrow ArH^+ + H. \tag{2}$$

Heterogeneous recombination of H atoms on the surface of the intermediate chamber and output nozzle could be a significant source of H_2 molecules, however [8]. We have estimated the possible H_2 production rate from this source using the approach developed previously for modelling such gas-surface processes at a substrate or a hot filament [12]. Consideration of the balance of gas phase H_2 loss reactions, diffusion processes in the thin gas-surface boundary layer and H atom abstraction and adsorption at the nozzle surface, suggests H_2 mole fractions, X_{H_2}, $\leqslant 0.06$ (averaged over the nozzle throat cross-section) for an initial 13.6% H_2 in Ar mixture. The chosen initial value for X_{H_2} does have a significant effect on the various C_yH_x species concentrations in the plume; we adopt a value $X_{H_2}=0$ in this initial 2D modelling study, which gives the highest calculated CH and C_2 number densities. The temperature dependence of the viscosity in the H/Ar gas mixture was explicitly included (e.g. $\sim 5\times10^{-4}$ and 8×10^{-4} g (cm s)$^{-1}$ at 1000 and 2000 K, respectively) [14]. The present calculations do not allow for diffusive transfer as a result of pressure gradients. Such processes [15], which induce preferential transfer of light species into regions of lower pressure, are expected to be particularly important in the shock wave region where they will alter the H and H_2 density profiles. Diffusive transfer could account for the anomalous H atom transport behaviour observed by Mazouffre et al. [8]. Another anomalous effect recognised by these workers [8]—very efficient recombination in a hydrogen plasma—is likely attributable to the fast ion conversion process (Eq. (3) [14]) in the arc channel.

$$H^+ + H_2 + H_2 \rightarrow H_3^+ + H_2 \quad (k_3 \sim 3\times10^{-29}\ \text{cm}^6\,\text{s}^{-1}). \tag{3}$$

The calculated gas temperature and flow velocities

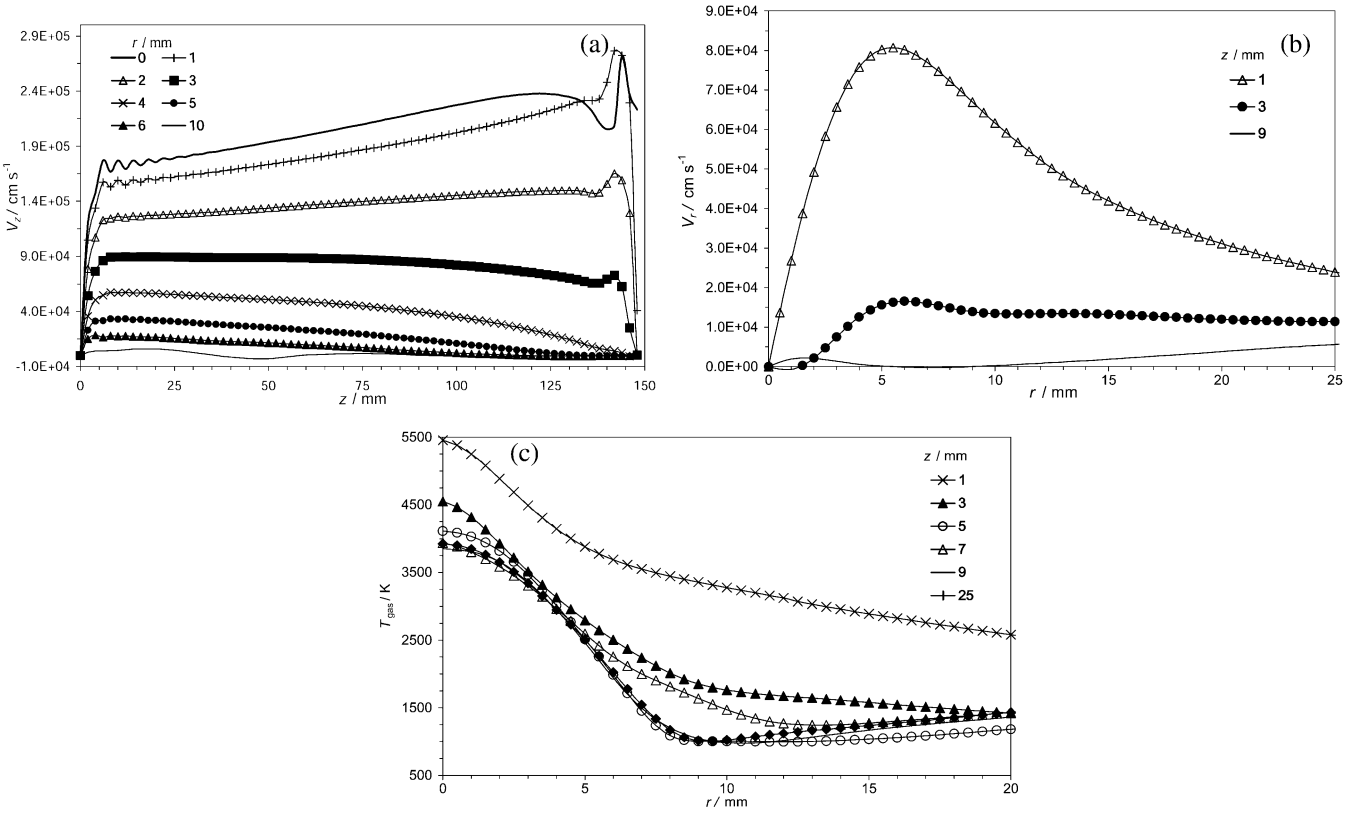

Fig. 2. Plots illustrating gas flow fields and gas temperature distributions derived in the 2D modelling: (a) plume propagation velocity (v_z) distributions, as a function of distance from the exit orifice of the N-torch ($z=150$ mm) to the substrate surface ($z=0$), at various r; (b) radial velocity (v_r) distributions at various perpendicular distances z from the substrate surface and (c) calculated radial dependence of T_{gas} for various z.

displayed in Fig. 2 clearly show a cylindrical hot plume with $T_{gas} \sim 3000-5000$ K and radius of approximately 0.5 cm, in good qualitative accord with previous C_2 optical emission measurements [5]. The calculated gas pressure, P, is not uniform throughout the reaction chamber: P exhibits a dramatic minimum in the shock region, and is calculated to be more than double the maintained base pressure (50 Torr) close to the substrate centre. Such pressure differentials aid the flow re-circulation discussed in previous studies of arc jet reactors [16,17]. The species density patterns obtained in the present 2D model calculations illustrate the important role of re-circulation flow in species transfer from the methane injection ring into the hot plume. Fig. 2b indicates typical transport velocities, $v_r \sim 2000$ cm s^{-1} in the main body of the reactor (i.e. away from the main plume and the substrate). The methane injection ring radius is $r=4$ cm, so the corresponding transport time is $t \sim r/v_r \sim 2$ ms. Many chemical transformations occur in the course of this transport. The initial step involves CH_4 decomposition via the reaction:

$$CH_4 + H \rightleftharpoons CH_3 + H_2. \quad (4)$$

Further H-shifting reactions lead to CH_x ($x=0-2$) radical production and simultaneous production of C_yH_x species by a variety of reactions [6], e.g.

$$C + C_yH_x \rightleftharpoons C_{y+1}H_{x-1} + H. \quad (5)$$

The families of H-shifting reactions of the type

$$C_yH_x + H \rightleftharpoons C_yH_{x-1} + H_2 \ (y=2-4) \quad (6)$$

are crucial for further redistribution amongst the various C_1H_x, C_2H_x, C_3H_x and C_4H_x hydrocarbon groups. Possible conversion of C_4H_x species to yet higher hydrocarbons is not allowed within the current chemical kinetics scheme. Note that the carbon balance within the reaction chamber is very non-uniform, changing from 0 at the nozzle to 0.2% in the plume just above the substrate. Because of re-circulation, the carbon balance in some of the off-plume regions of the reaction chamber reaches ~1%—i.e. some 2.5 times high than the equilibrium value of 0.4%. (Recall that the CH_4 flow rate (60 sccm) is 0.4% of the total flow rate.)

Off-plume processes such as those identified above determine the various hydrocarbon concentrations in the annular transition layer ($r \sim 0.5-1$ cm) bounding the hot

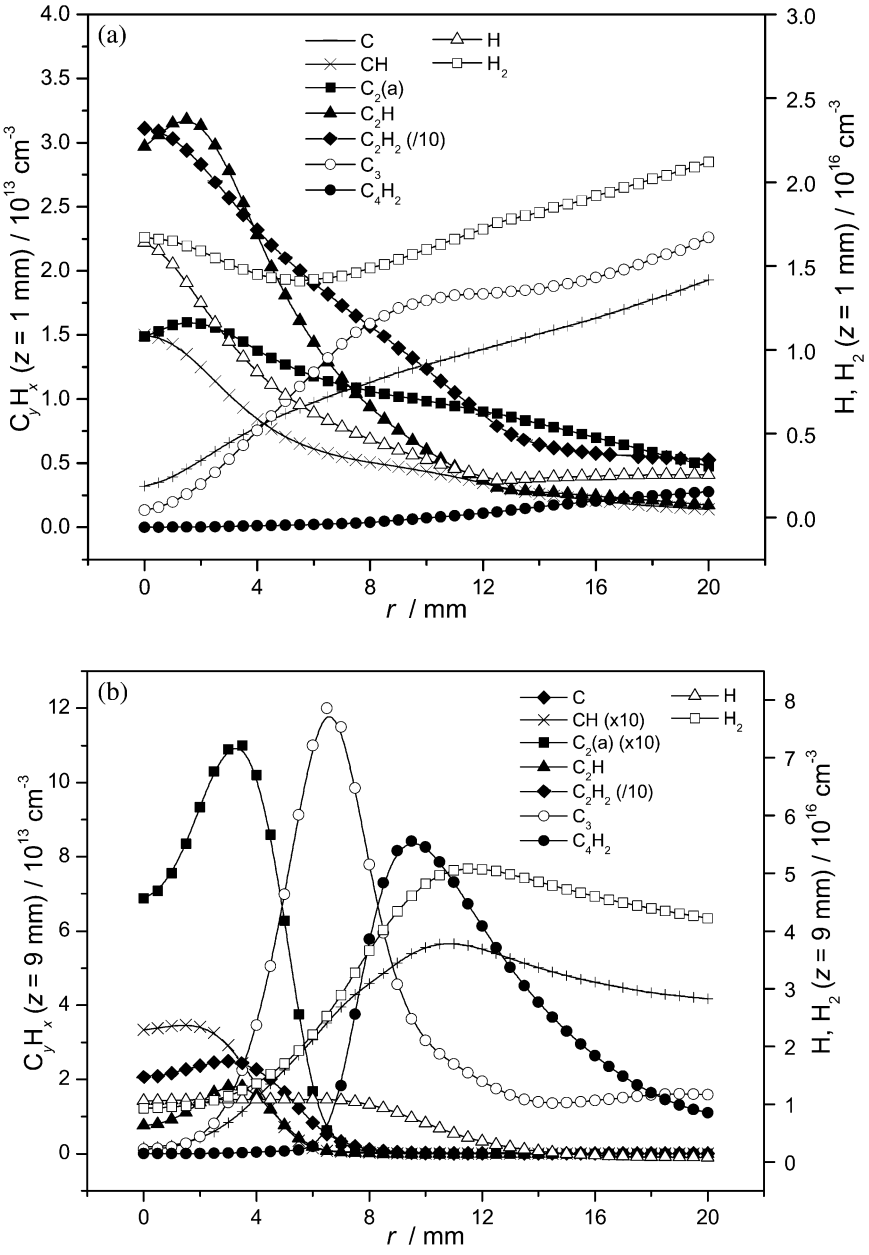

Fig. 3. Calculated radial number density distributions of H atoms and H_2 (right hand axis) and various of the key C_yH_x species (scale on left hand axis), at $z=1$ mm (a) and 9 mm (b).

plume ($r<0.5$ cm). Hydrocarbon incorporation into the plume occurs mainly by diffusive transfer. As Fig. 3 shows, only species with the highest diffusion coefficients (e.g. C atoms and CH radicals) have time to develop a radial profile that maximizes at $r=0$ during the mean time of flight from the nozzle to the substrate (i.e. $t\sim0.08$ ms at $r=0$, but rising to ~0.4 ms when $r=5$ mm). The calculated number density distributions of heavier hydrocarbons (e.g. C_3H_x, C_4H_x) thus display an obvious minimum at $r=0$. Such trends are reinforced by the fact that t is too short for significant production of C_3H_x and higher hydrocarbons from the CH_x and C_2H_x species that do manage to diffuse into the small r region. We note that the CH, C_2 and C_3 radical densities observed in experimental studies of another DC arc jet reactor [18] show radial trends that accord very well with these model outputs.

As mentioned earlier, previous analyses of individual Doppler linewidths within the $C_2(d–a)$ spectrum suggested a substantial rise in T_{gas} within 5 mm of the substrate [2]. Such a conclusion appears inconsistent with the Boltzmann analysis of the $C_2(d–a)$ spectrum recorded at $z=2$ mm (Fig. 1), which reveals no obvious increase in T_{rot} at small z. This apparent dichotomy can

be explained by the present modelling. As Fig. 2c shows, T_{gas} is indeed calculated to peak at $z \rightarrow 0$. However, the plume flares out along r close to the substrate (Fig. 2b). The length of the absorbing column of C_2 (and CH) radicals at small z is thus increased, as can be seen by comparing their respective r dependent profiles calculated at $z = 1$ mm (Fig. 3a) and 9 mm (Fig. 3b). Species at large r will have a lower associated T_{gas}, thereby lowering the 'average' temperature deduced by a column measurement. This is exacerbated further in the case of the heavier C_2 radical for which, as Fig. 3a shows, the number density profile is predicted to exhibit a local minimum at $z = 0$. Thus, the 'average' temperature associated with the calculated C_2 number density distribution is relatively constant, at $\sim$3550 K, for all $z \leqslant 5$ mm, and then declines to $\sim$3350 K at larger z. As Fig. 3a and b show, a larger fraction of the calculated CH density is to be found in the small r, small z region where T_{gas} is predicted to be highest. Not surprisingly, therefore, somewhat higher 'average' temperatures would be predicted from column measurements of CH: $\sim$3500 K for $z > 5$ mm, rising to almost 4000 K at $z = 1$ mm. Experiment mimics all of these model predictions, except for the gas temperatures obtained at small z derived from the original $C_2(d–a)$ Doppler lineshape analysis. However, the evident broadening of the $C_2(d–a)$ transitions measured at small z can also be understood in terms of the local plume flaring revealed in Fig. 2b. We have attempted to replicate the experimentally measured lineshapes using r dependent gas velocities, temperatures and C_2 number density profiles from the 2D (r, z) calculations. Doppler broadened line profiles for the appropriate local gas temperatures (from the 2D model) were shifted in accord with the local velocity component along the laser propagation axis, and summed with weightings corresponding to the calculated local $C_2(a)$ densities and T_{gas} values. The resultant profiles were fitted to Gaussian functions, which were found to mimic the observed trend of increasing FWHM as $z \rightarrow 0$. We conclude, therefore, that the observed increase in linewidth at small z is mainly a consequence of plume flaring and the consequent re-direction of the gas flow perpendicular to the arc jet axis rather than any localised heating effect.

4. Film growth rates

The high deposition rates ($\sim$100 μm h^{-1} for our base reactor parameters) achieved in this and other DC arc jet reactors can be rationalised in the light of the calculated radical fluxes incident on the substrate surface. In the DC arc jet reactor under study the calculated ratio of atomic to molecular hydrogen number densities, $[H]/[H_2]$, just above the substrate is $\sim$1. This value should be compared with that found in traditional low power hot filament or microwave plasma enhanced CVD reactors, where $[H]/[H_2] \sim 0.001–0.05$ [7]. In contrast to these more traditional diamond CVD conditions, therefore, dissociative adsorption of H_2 (Eq. (7)) will be relatively unimportant under DC arc jet growth conditions, and the free radical site fraction, f^*, in these latter conditions will depend largely on the atomic hydrogen abstraction and adsorption reactions Eqs. (7) and (8):

$$H + CH \rightleftharpoons C^* + H_2 \tag{7}$$

$$H + C^* \rightleftharpoons CH \tag{8}$$

CH and C* represent hydrogen terminated and non-terminated surface sites and $f^* = C^*/(C^* + CH) = k_7/(k_7 + k_8)$. Assuming a substrate temperature $T_s = 1200$ K and respective rate coefficients $k_7 = 3.2 \times 10^{-12} T_{ns}^{0.5} \exp(-3430/T_s)$ (cm^3 s^{-1}) and $k_8 = 9.6 \times 10^{-13} T_{ns}^{0.5}$ (cm^3 s^{-1}) [19] (where T_{ns} is the gas temperature just above the substrate), we obtain $f^* \sim 0.16$. The deposition rate depends on the adsorption rates of hydrocarbon species at the radical sites, i.e.

$$C_yH_x + C^* \rightleftharpoons C–C_yH_x \tag{9}$$

Assuming a value of $k_9 = 2.4 \times 10^{-13} T_{ns}^{0.5}$ (cm^3 s^{-1}) for these rate coefficients—typical for a barrierless radical recombination process [19]—we arrive at an upper limit estimate for the diamond growth rate, G [6]:

$$G\ (\mu\text{m h}^{-1}) = 6 \times 10^{-15} T_{ns}^{0.5} \sum ([C_yH_x]y), \tag{10}$$

where $[C_yH_x]$ is the concentration of a given hydrocarbon radical just above the substrate. Fig. 3a showed that the major contributors to the sum $\sum([C_yH_x]y)$ impinging on the substrate are C_2H, C, CH, C_2 and C_3 species. It is worth sounding a note of caution here. The pre-multiplier in Eq. (10) is appropriate for an incident C atom flux, but would generally be considered to overestimate the contribution that heavy hydrocarbons make to G [19]. Conversely, however, we might argue that the G value derived using Eq. (10) might need to be increased by a factor 1.5–2 in recognition of the disturbance of the thermal velocity distributions of the various participating species by the high gas flow velocity in the plume ($v_z \sim 1$ km s^{-1}). Either way, however, to obtain G values $\sim$100 μm h^{-1} given the calculated gas temperatures ($T_{ns} > 4000$ K, Fig. 2c) and species concentrations at $z \sim 1$ mm (Fig. 3a), it is necessary to assume a value close to the upper limit of $\sum([C_yH_x]y)$ that can be achieved by involving all of the above species. As in previous modelling of diamond growth from thermal plasmas [20], the present calculations also find significant concentrations of CH_2

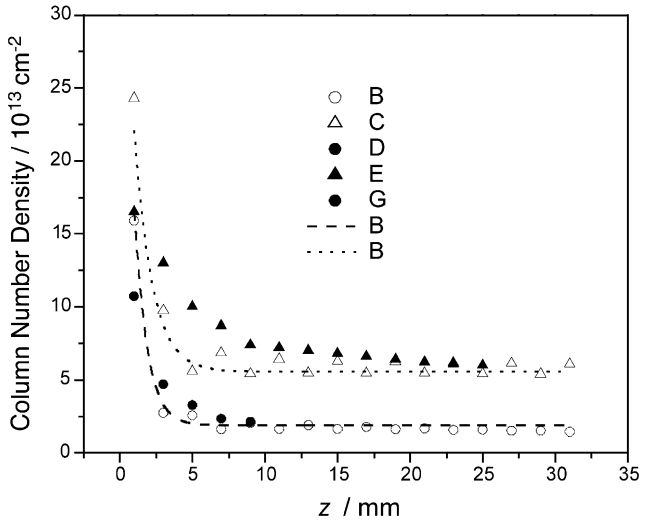

Fig. 4. $C_2(a)_{v=0}$ and $CH(X)_{v=0}$ radical column densities in a CH_4 (60 sccm)/H_2 (1.8 slm)/Ar (12.15 slm) gas mixture operating at an input power of ~6.5 kW obtained from measured (by CRDS) absorbances, at various z (solid symbols) and the corresponding quantities derived from the 2D modelling (open symbols, together with dashed lines to guide the eye). Note that the revision of the gas temperatures at small z demonstrated in this work has led to a downward revision of the experimental column densities at $z=1$ from those given in Ref. [2].

($\sim 8\times10^{12}$ cm^{-3}) and CH_3 radicals ($\sim 2\times10^{12}$ cm^{-3}) developing in a thin (~1 mm) layer just above the substrate. All of the above-mentioned C_yH_x species could, in principle, contribute to the carbon deposition rate in the Bristol DC arc jet reactor. Indeed, given the high growth rates observed, it seems likely that all of the more abundant carbon containing radical species (i.e. C_2H, C, CH, C_2 and C_3), at least, must be contributing to material growth.

5. Comparison between experimental and calculated CH and $C_2(a)$ number densities

The availability of T_{gas} (Fig. 2c) and species number density (Fig. 3a and b) profiles from the 2D (r, z) modelling allows calculation of column densities that can be compared directly with the experimental CRDS measurements. Fig. 4 presents such a comparison, for the case of $C_2(a)_{v=0}$ and $CH(X)_{v=0}$ radical column densities (cm^{-2}) at different distances from the substrate, in a CH_4 (60 sccm)/H_2 (1.8 slm)/Ar (12.15 slm) gas mixture operating at an input power of ~6.5 kW. The calculated column densities of radicals specifically in their $v=0$ levels were obtained as an integral over the line of sight through the reactor of the calculated $C_2(a)$ and $CH(X)$ number densities each divided by the appropriate vibrational partition function $q=1/[1-\exp(-\Delta\varepsilon/T(r, z))]$, where $\Delta\varepsilon$ is the vibrational quantum (1618 and 2733 cm^{-1} for C_2 and CH, respectively). Note that the z dependent oscillations—most evident in the $C_2(a)$ column density plot—are an artefact arising from the use of the central difference numerical scheme. The route to deriving the total column density of a chosen target species from an experimental determination of the absorption coefficient of any given transition is explained in detail in Ref. [2]. It requires assumption of a species temperature, which determines the fraction of the total population distribution that contributes to a given line absorption. As we have seen above, the original $C_2(a)$ and $CH(X)$ number density estimates at small z assumed excessive 'average' temperatures [2]. The experimental column densities at $z<5$ mm have thus been re-calculated assuming the (lower) average temperatures given in Section 3 above. Clearly, the effect is fairly small, since neither the rotational or vibrational partition functions are much affected by such a minor change in a large temperature but, equally clearly, the experimental and modelled column densities for both $C_2(a)$ and $CH(X)$ are in almost quantitative agreement. Further evidence for the validity of the modelling comes from comparing experimental and model C_2H_2 column densities. Continuous wave CRDS measurements of C_2H_2 in the DC arc jet reactor operating with a reduced CH_4 flow (15 sccm) but otherwise equivalent gas feed and input power conditions yielded average values for T_{gas} and C_2H_2 concentration of ~550 K and 1.2×10^{14} cm^{-3}, respectively, independent of z, in the range $1<z<15$ mm [21]. The low average T_{gas} value was rationalised by assuming that C_2H_2 is widely distributed throughout the reactor, extending well beyond the regions of highest thermal activation as a result of diffusion processes. The present 2D (r, z) modelling confirms these suppositions, yielding radially averaged C_2H_2 number densities of $\sim 2.1\times10^{14}$ cm^{-3} (at $z=1$ mm) and $\sim 4.0\times10^{14}$ cm^{-3} ($z=9$ mm), for a 60 sccm CH_4 flow that agree well with the experimental value (after scaling for the reduced (15 sccm) CH_4 flow employed), and an 'average' T_{gas} value that is in similarly good accord with that found experimentally.

Acknowledgments

We are grateful to Element Six Ltd (formerly De Beers Industrial Diamonds) for the loan of the DC arc plasma jet system, to the EPSRC for equipment funding, post doctoral support (JAS) and a project studentship (CJR), the Royal Society for a Joint Project Grant that enables the Bristol–Moscow collaboration, and to NATO for the awards of SfP grant N974354 (YAM) and JSTC.RCLG.979556 (MNRA).

References

[1] M.A. Cappelli, T.G. Owano, in: B. Dischler, C. Wild (Eds.), Low Pressure Synthetic Diamond, Springer, Berlin, 1998, pp. 59–84.

[2] J.B. Wills, J.A. Smith, W.E. Boxford, J.M.F. Elks, M.N.R. Ashfold, A.J. Orr-Ewing, J. Appl. Phys. 92 (2002) 4213.
[3] M.D. Wheeler, S.M. Newman, A.J. Orr-Ewing, M.N.R. Ashfold, J. Chem. Soc. Faraday Trans. 94 (1998) 337.
[4] G. Berden, R. Peeters, G. Meijer, Int. Rev. Phys. Chem. 19 (2000) 565.
[5] J.A. Smith, K.N. Rosser, H. Yagi, M.I. Wallace, P.W. May, M.N.R. Ashfold, Diamond Relat. Mater. 10 (2001) 370.
[6] Y.A. Mankelevich, N.V. Suetin, M.N.R. Ashfold, et al., Diamond Relat. Mater. 12 (2002) 383.
[7] J.A. Smith, Ph.D. Thesis, University of Bristol, 2002.
[8] S. Mazouffre, P. Vankan, R. Engeln, D.C. Schram, Phys. Plasmas 8 (2001) 3824.
[9] M.E. Green, C.M. Western, J. Chem. Phys. 104 (1996) 848, PGOPHER spectral simulation program written by C.M. Western. A summary of the program and the Hamiltonian used is given in.
[10] G.M. Lloyd, P. Ewart, J. Chem. Phys. 110 (1999) 385.
[11] C.V.V. Prasad, P.F. Bernath, Astrophys. J. 426 (1994) 812.
[12] Y.A. Mankelevich, A.T. Rakhimov, N.V. Suetin, Diamond Relat. Mater. 5 (1996) 888.
[13] R. Engeln, S. Mazouffre, P. Vankan, D.C. Schram, N. Sadeghi, Plasma Sources Sci. Technol. 10 (2001) 595.
[14] I.S. Grigoriev, E.Z. Meilihov (Eds.), Hand-book 'Physical Data', Energoatomizdat, Moscow, 1991, p. 365.
[15] B.V. Alekseev, A.M. Grishin, Phys. Gas Dynamics React. Media, Moscow, ''High School'' (Publishing House), 1985, p. 120 (in Russian).
[16] R.F.G. Meulenbroeks, R.A.H. Engeln, M.N.A. Beurskens, et al., Plasma Sources Sci. Technol. 4 (1995) 74.
[17] W. Juchmann, J. Luque, J.B. Jeffries, Appl. Optics 39 (2000) 3704.
[18] J. Luque, W. Juchmann, J.B. Jeffries, J. Appl. Phys. 82 (1997) 2072.
[19] S. Skokov, B. Weiner, M. Frenklach, J. Phys. Chem. 99 (1995) 5616.
[20] B.W. Yu, S.L. Girshick, J. Appl. Phys. 75 (1994) 3914.
[21] J.B. Wills, M.N.R. Ashfold, A.J. Orr-Ewing, Y.A. Mankelevich, N.V. Suetin, Diamond Relat. Mater. 12 (2003) 1346.